Photometry, Period Study, and Light Curve Modeling of the HADS Variables BN Trianguli and V488 Geminorum

Kevin B. Alton
UnderOak Observatory, 70 Summit Avenue, Cedar Knolls, NJ 07927; kbalton@optonline.net

Received August 30, 2022; revised November 25, 2022; accepted December 2, 2022

Abstract Multi-bandpass (BVI_c) CCD-derived photometric data were acquired from BN Tri and V488 Gem (ATO J106.2184+10.4567) at Desert Blooms Observatory (DBO). Both of these pulsating variables are classified as high amplitude δ Scuti-type systems. Analysis of precise time-series light curve data from each target was accomplished using discrete Fourier transformation (DFT) which in both cases revealed a dominant fundamental mode (f_0) of oscillation along with associated harmonics. Furthermore, BN Tri exhibited two other statistically meaningful but low amplitude independent pulsation modes, while V488 Gem may possess up to four other independent oscillations. New times of maximum (ToMax) produced from both targets were combined with other ToMax timings mined from other sources (SuperWASP, TESS, and AAVSO-VSX) in order to update their corresponding linear ephemerides. Preliminary evidence suggests a secular increase in the fundamental oscillation period of BN Tri between 1999 and 2021. In contrast, secular analysis of the fundamental pulsation period for V488 Gem (ATO J106.2184+10.4567) revealed a sinusoidal-like variation in the pulse timing differences. These residuals, believed to result from a light-travel time effect (LiTE), were fit using simplex optimization. The resulting LiTE simulation suggested that V488 Gem is a binary system with a stellar-sized object in an eccentric orbit (7.91 ± 0.09 y). The evolutionary status, age, and physical nature of both HADS variables were investigated using the PAdova and TRieste Stellar Evolution Code for generating stellar tracks and isochrones. The totality of results including residence in the Galactic thin disk, near solar metallicity, mass predictions, and effective temperature estimates firmly support classification for both stars as high amplitude \delta Scuti-type variables.

1. Introduction

High amplitude δ Scuti stars, hereafter HADS, represent a very small percentage (<1%) of all δ Sct variables (Lee *et al.* 2008). They commonly oscillate (ΔV > 0.1 mag) via low-order single or double radial pulsation modes (Poretti 2003a; Poretti 2003b; Niu *et al.* 2013; Niu *et al.* 2017) driven by the κ-mechanism (opacity bump) resulting from partial ionization of He II (Pamyatnykh 1999). Many (~40%) are double mode pulsators exhibiting simultaneous pulsations in the fundamental and the first overtone mode with amplitudes generally higher in the fundamental mode (McNamara 2000). HADS variables have traditionally been divided according to metallicity relative to the Sun where [Fe/H] is defined as zero. The metal-poor ([Fe/H] << 0) group is classified as SX Phe-like stars, based on the prototype SX Phoenicis. Ostensibly they have shorter periods (0.02 < P < 0.125 d) and lower masses (~1.0–1.3 $M_\odot$) than related HADS variables possessing near solar metal abundance (McNamara 2011). SX Phe stars frequently reside in globular clusters (GC), which are ancient collections of Population II stars. The majority of these pulsators are classified as blue straggler stars, paradoxically appearing much younger than their GC cohorts. Balona and Nemec (2012) proposed that it is not possible to differentiate between δ Sct and field SX Phe variables based on pulsation amplitude, the number of pulsation modes, period, or even metallicity (Garg *et al.* 2010). Much more sensitive space instruments like the National Aeronautics and Space Administration's (NASA) Kepler Mission (Gilliland *et al*. 2010; Guzik 2021), the European Space Agency's (ESA) Convection, Rotation and planetary Transits (CoRoT) Mission (Baglin 2003), and the Canadian Microvariability and Oscillations of STars (MOST) Mission (Walker *et al.* 2003) have found many examples that violate the traditional differentiation between HADS and SX Phe pulsators. Balona and Nemec (2012) further contend that the evolutionary status of each star is the only way to distinguish between these two classes.

An additional classification scheme for δ Scuti stars was proposed by Qian *et al.* (2018) wherein two distinct groups of δ Scuti stars that fundamentally differed in effective temperature were uncovered from the Large Sky Area Multi-Object Fiber Spectroscopic Telescope (LAMOST) survey (Zhao *et al.* 2012). One group was identified as normal δ Scuti stars (NDSTs) when T_{eff} ranged between 6700–8500 K, while the other was defined as unusual and cool variable stars (UCVs) with T_{eff} values less than 6700 K. A more narrow fundamental pulsation period range (0.09–0.22 d) coupled with being slightly metal poor (–0.25 ≤ [Fe/H] ≤ 0.0) further differentiates the UCVs from the NDST group. Furthermore, once UCV stars were removed from the analyses, empirically based temperature-period, log g-period, and metallicity-period relationships could be derived for NDSTs.

Herein, a photometric investigation of BN Tri and V488 Gem (ATO J106.2184+10.4567) is described which includes Fourier deconvolution of their light curves to derive significant pulsation mode(s) along with an evolutionary analysis using PARSEC models (Bressan *et al.* 2012). CCD-derived photometric data for BN Tri (GSC 1763-0477) were first acquired from the ROTSE-I survey between 1999 and 2000 (Akerlof *et al.* 2000; Woźniak *et al.* 2004; Gettel *et al.* 2006) and later from the Catalina Sky (Drake *et al.* 2014) and SuperWASP (Pollacco *et al.* 2006) surveys. Khruslov (2007) initially identified this pulsating variable as a δ Scuti-type system based on data from the ROTSE-I survey. Later on (2019) light curves for BN Tri derived from time-series exposures (120 s) were produced by the TESS Science Processing Operations Center (TESS-SPOC) (Jenkins *et al.* 2016).

Evidence for the variability of V488 Gem can be found in light curve data (2002–2009) from the sparsely-sampled All Sky Automated Survey (ASAS) (Pojmański 2000; Pojmański *et al.* 2005) and the ASAS-SN (2014–2018) survey (Jayasinghe *et al.* 2018). Time-series light curve measurements from V488 Gem were also mined from the AAVSO International Database (Kafka 2021) and TESS-SPOC archives (Jenkins *et al.* 2016).

No reported times of maximum (ToMax) for BN Tri and only four for V488 Gem (Wils *et al.* 2013; Wils *et al.* 2014) have been found in the literature. This paper marks the first detailed multi-bandpass, secular, and evolutionary study for both HADS variables.

2. Observations and data reduction

Precise time-series images were acquired at Desert Blooms Observatory (DBO, USA, 31.941 N, 110.257 W) using a QSI 683 wsg-8 CCD camera mounted at the Cassegrain focus of a 0.4-m Schmidt-Cassegrain telescope. A Taurus 400 (Software Bisque) equatorial fork mount allowed continuous operation without the need to perform a meridian flip. The image (science, darks, and flats) acquisition software (TheSkyX Pro Edition 10.5.0; Software Bisque 2019) controlled the main and integrated guide cameras.

This focal-reduced (f/7.2) instrument produces an image scale of 0.76 arcsec/pixel (bin =2 × 2) and a field-of-view (FOV) of 15.9 × 21.1 arcmin. The CCD camera is equipped with B, V, and I_c filters manufactured to match the Johnson-Cousins Bessell prescription. Computer time was updated immediately prior to each session. Dark subtraction, flat correction, and registration of all images collected at DBO were performed using AIP4Win v2.4.1 (Berry and Burnell 2005). Instrumental readings were reduced to catalog-based magnitudes using the AAVSO Photometric All-Sky Survey (APASS) star fields (Henden *et al.* 2009; Henden *et al.* 2010; Henden *et al.* 2011; Smith *et al.* 2011) built into MPO Canopus v10.7.1.3 (Minor Planet Observer 2010). When necessary, I_c values were estimated from B, V, r', and i'-mag values according to Jester *et al.* 2005. The identities (HST Guide Star Catalog, Version GSC-ACT), Gaia DR2 J2000 coordinates and APASS color indices (B–V) for each ensemble of comparison stars used for differential aperture photometry are provided in Table 1. Since all program stars share a relatively small FOV, differential atmospheric extinction was ignored, while data from images taken below 30° altitude (airmass > 2.0) were excluded. All photometric data acquired from BN Tri and V488 Gem at DBO can be retrieved from the AAVSO International Database (Kafka 2021).

Uncertainty in comparison star measurements, calculated according to the so-called "CCD Equation" (Mortara and Fowler 1981), typically stayed within ±0.007 mag for V- and I_c- and ±0.010 mag for B-passbands. The identity, J2000 coordinates, and color indices (B–V) for these stars are provided in Table 1. AAVSO finder charts for BN Tri (Figure 1) and V488 Gem (Figure 2) are centered around each target along with a corresponding ensemble of comparison stars used for differential aperture photometry.

Time-of-Maximum (ToMax) light values and associated uncertainties from data acquired at DBO and those mined from AAVSO-VSX, TESS, and SuperWASP were calculated according to Andrych and Andronov (2019) and Andrych *et al.* (2020) using the "Polynomial Fit" routine in the program MAVKA (https://uavso.org.ua/mavka/). Simulation of extrema was automatically optimized by finding the most precise degree (α) and best fit algebraic polynomial expression.

Long-term or secular changes in the fundamental pulsation period can sometimes be revealed by plotting the difference between the observed maximum light times and those predicted by a reference epoch against cycle number. These pulsation timing differences (PTD) vs. epoch were fit using scaled Levenberg-Marquardt algorithms (QtiPlot 0.9.9-rc9; https://www.qtiplot.com/). Results from these analyses are separately discussed for each HADS variable in the subsections (3.1 and 3.2) below.

No medium-to-high resolution classification spectra were found in the literature for either variable. As such, the effective temperature (T_{eff}) of each star has been estimated using color index (B–V) data acquired at DBO and from the 2MASS survey. 2MASS J and K values were transformed to (B–V) (http://brucegary.net/dummies/method0.html). In both cases, interstellar extinction (A_V) was calculated (E(B–V) × 3.1) using the reddening values (E(B–V)) estimated from Galactic dust map models reported by Schlafly and Finkbeiner (2011). Additional effective temperature values were mined from the Gaia DR2 (http://vizier.u-strasbg.fr/viz-bin/VizieR?-source=I/345/gaia2), LAMOST DR5 (http://dr5.lamost.org/search), and TESS (https://exofop.ipac.caltech.edu/tess/) websites. The mean T_{eff} value derived from all sources (Table 2) indicates an effective temperature (7371 ± 186 K) for BN Tri that probably ranges in spectral class between A8V and F0V. The reader should be aware of dangers associated with adopting a single T_{eff} value for a pulsating variable. With the exception of light curves acquired at DBO it is not known when T_{eff} measurements were made during each pulsation cycle. For example, with BN Tri (Figure 3) the largest difference between maximum and minimum light is observed in the blue passband (ΔB = 0.24 mag), followed by V (ΔV = 0.18 mag) and finally the smallest difference detected in infrared (ΔI_c = 0.11 mag). Plotting (B–V) against phase (Figure 4) shows significant color index change (Δ = 0.07 mag) going from maximum ((B–V)≃0.21 mag) to minimum light ((B-V)≃0.28 mag). This corresponds to a T_{eff} which ranges between 7650 and 7363 K.

Similarly, dereddened color indices ($(B–V)_0$) for V488 Gem gathered from different sources are also listed in Table 2. The mean value (7129 ± 202 K) corresponds to a star that likely ranges in spectral class between A9V and F1V. An examination of the light curves acquired at DBO reveals that the largest difference between maximum and minimum light is observed in the blue passband (ΔB = 0.64 mag), followed by V (ΔV = 0.48 mag) and finally the smallest difference detected in infrared (ΔI_c = 0.29 mag). Plotting (B–V) against phase (Figure 5) shows significant color index change (Δ = 0.21 mag) going from maximum ((B–V)≃0.15) to minimum light ((B–V)≃0.36) where V488 Gem is least bright. These values correspond to an effective temperature which ranges between 7893 and 7023 K.

Table 1. Astrometric coordinates (J2000), V-mags and color indices (B–V) for BN Tri, V488 Gem and their corresponding stars used for ensemble aperture photometry.

Star Identification	*R.A. (J2000) h m s*	*Dec. (J2000) ° ′ ″*	*V-mag*[a]	*(B–V)*[a]
BN Tri	01 54 58.043	+29 47 37.06	12.010	0.302
GSC 1763-0205	01 55 26.596	+29 51 53.40	12.395	0.553
GSC 1763-0151	01 55 44.066	+29 54 05.17	11.524	0.563
GSC 1763-1011	01 55 07.094	+29 54 44.61	12.172	0.684
GSC 1763-0859	01 55 45.534	+29 43 45.11	11.518	0.509
V488 Gem	07 04 52.410	+10 27 24.20	12.596	0.533
GSC 7530-1915	07 04 29.567	+10 20 43.61	10.838	0.397
GSC 7530-1677	07 04 25.243	+10 17 55.43	12.378	0.417
GSC 7530-1473	07 05 21.822	+10 18 48.90	10.869	0.483
GSC 7530-2574	07 05 28.505	+10 25 32.52	12.183	0.407
GSC 7530-1301	07 05 06.695	+10 25 53.10	11.776	0.634

[a] *V-mag and (B–V) for comparison stars derived from APASS database described by Henden* et al. *(2009, 2010, 2011) and Smith* et al. *(2011).*

3. Results and discussion

Results and detailed discussion about the determination of ephemerides are individually provided for BN Tri and V488 Gem in this section. Thereafter, deconvolution of pulsation period(s) using a Discrete Fourier Transform (DFT) routine featured in Period04 (Lenz and Breger 2005) are separately examined. Finally, preliminary estimates for mass ($M_\odot$) and radius ($R_\odot$), along with corresponding calculations for luminosity ($L_\odot$), surface gravity (log (g)), and bolometric magnitude (M_{bol}), are derived from study observations and predictions based upon evolutionary modeling.

3.1. BN Tri

3.1.1. Photometry and ephemerides

Photometric values in B (n = 290), V (n = 289), and I_c (n = 278) acquired between 2020 December 1 and 2021 November 29 were each period-folded producing light curves in three passbands (Figure 3). Included in these determinations were 45 new ToMax values which are summarized in Table 3. BN Tri was also imaged during the SuperWASP survey (Pollacco *et al.* 2006), which provided a rich source of photometric data taken (30-s exposures) at modest cadence that repeats every 9 to 12 min. In some cases (n = 69) these measurements taken between 2004 and 2006 were amenable to extrema estimation using MAVKA.

Although primarily designed to capture very small host star brightness changes during an exoplanet transit, the TESS Mission (Ricker *et al.* 2015; Caldwell *et al.* 2020) also provides a wealth of light curve data for many variable stars. The four TESS cameras produce a combined FOV of 24° × 96°. Each ecliptic hemisphere is divided into 13 partially overlapping sectors (24° × 96°) that extend from 6° latitude to the ecliptic pole. Each sector is then continuously observed for 27.4 days (two spaceship orbits), with the camera boresight pointing at ± 54° latitude or approximately antisolar. To observe the next sector, the FOV is shifted eastward in ecliptic longitude by about 27°. Each hemisphere takes one year to image with the all-sky survey completed in ~2 y. A pre-selected number of dwarf

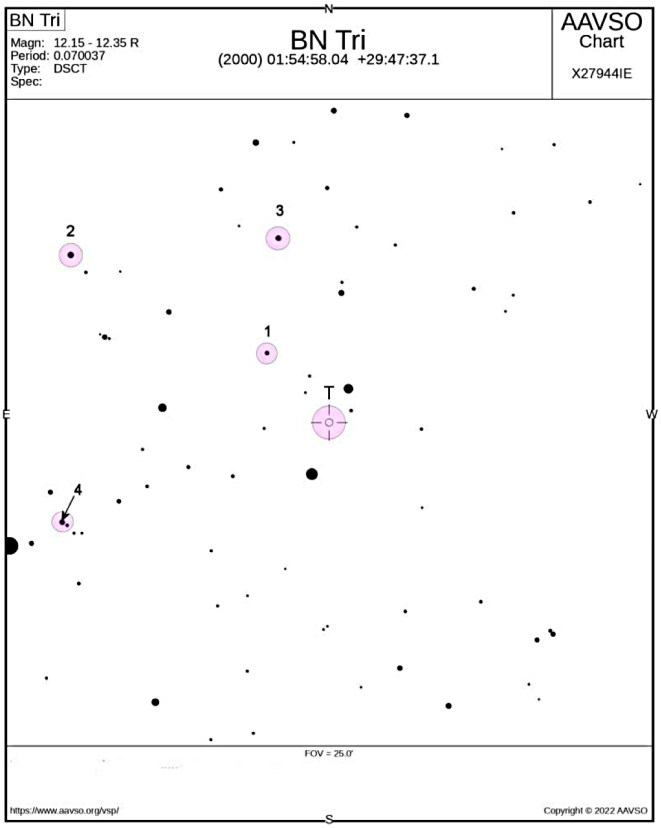

Figure 1. Finder chart for target (T) variable BN Tri (center) also showing the comparison stars (1–4) used for aperture-derived ensemble photometry.

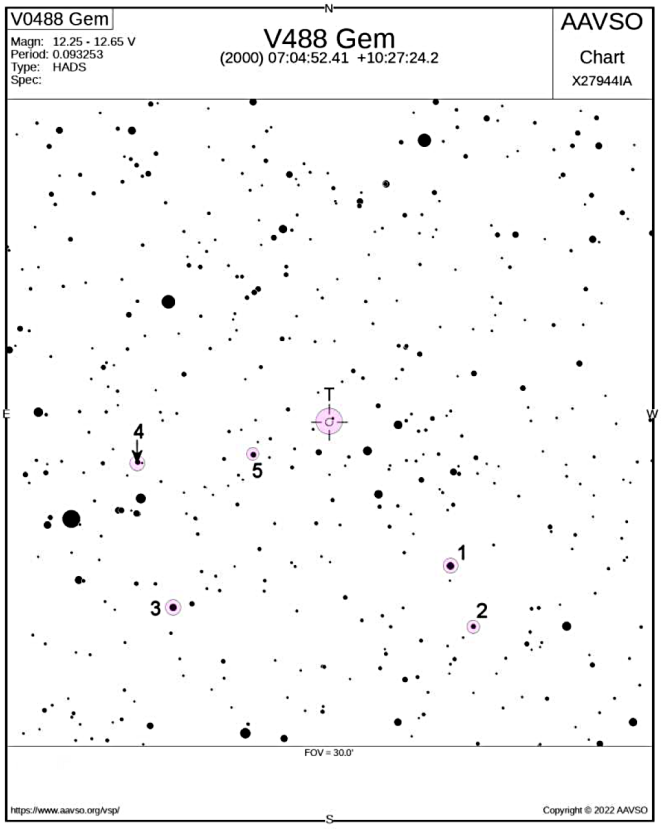

Figure 2. Finder chart for target (T) variable V488 Gem (center) also showing the comparison stars (1–5) used for aperture-derived ensemble photometry.

Table 2. Derivation of the eective temperature (T_{eff}) of BN Tri and V488 Gem based upon estimates from multiple sources.

	2MASS	*DBO*	*Gaia DR2*[a]	*LAMOST DR5*[b]	*TESS*[c]	*Mean*
BN Tri						
$(B–V)_0$[d]	0.307 (44)	0.246 (20)	—	—	—	—
T_{eff}[e] (K)	7181 (225)	7504 (110)	7556 -204+203	-	7243 (152)	7371 (186)
Spectral Class[f]	A9V-F1V	A7V-A9V	A7V-A9V	—	A9V-F0V	A8V-F0V
V488 Gem						
$(B–V)_0$[d]	0.356 (48)	0.259 (39)	—	—	—	—
T_{eff}[e] (K)	6935 (309)	7434 (213)	7216 -122+149	7085 (58)	6977 (166)	7129 (202)
Spectral Class[f]	F0V-F4V	A8V-F0V	A9V-F1V	F0V-F2V	F0V-F4V	A9V-F1V

[a] *Gaia Collab. (2016, 2018).* [b] *Zhao* et al. *(2012).* [c] *https://exofop.ipac.caltech.edu/tess/ .* [d] *Intrinsic $(B–V)_0$ determined using E(B–V) reddening value (BN Tri = 0.0762 ± 0.0017 and V488 Gem = 0.0828 ± 0.0019); T_{eff} interpolated from Pecaut and Mamajek (2013).* [e] *Mean T_{eff} values adopted for evolutionary modeling.* [f] *Spectral class range estimated from Pecaut and Mamajek (2013).*

Table 3. Sample table for BN Tri times-of-maximum (November 15, 1999–November 29, 2021), cycle number and fundamental pulsation timing difference (PTD) between observed and predicted times derived from the updated linear ephemeris (Equation 1).

HJD 2400000+	*HJD Error*	*Cycle No.*	*PTD*	*Ref.*
51497.8616	0.0010	–114942	0.00386	1
53200.6897	0.0006	–90628	0.00073	2
53203.7040	0.0007	–90585	0.00350	2
58767.7723	0.0002	–11138	0.00023	4
58767.8422	0.0002	–11137	0.00010	4
58767.9119	0.0002	–11136	–0.00026	4

References: (1) NSVS (Akerlof et al. *2000; Wozniak* et al. *2004; Gettel* et al. *2006); (2) SuperWASP (Polacco* et al. *2006); (4) TESS-SPOC (Jenkins* et al. *2016). Full table available at: ftp://ftp.aavso.org/public/datasets/3852-Alton-bntri.txt. All references relevant to the fulltable that appears on the AAVSO ftp site are included in the References section of this article and in the full ftp table.*

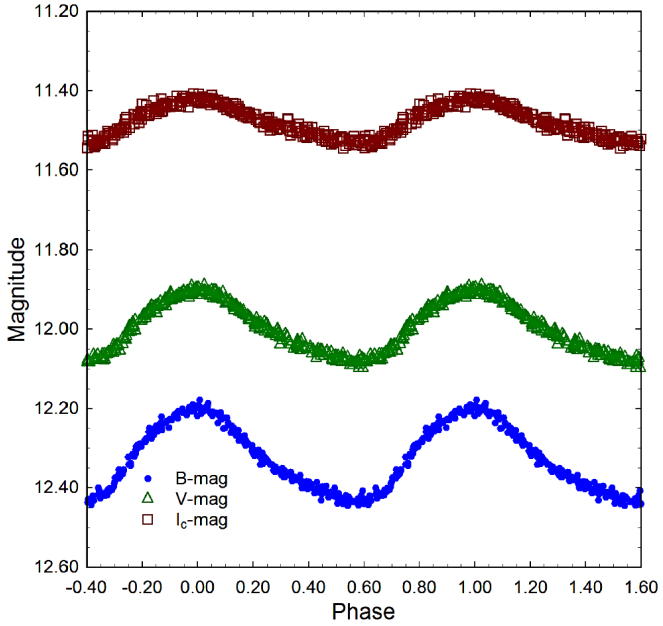

Figure 3. Period (0.070035 ± 0.000002 d) folded CCD light curves for BN Tri produced from photometric data obtained between 2020 December 1 and 2021 November 29 at DBO. The top (I_c), middle (V), and bottom curve (B) shown above were reduced to APASS-based catalog magnitudes using MPO Canopus.

Table 4. Fundamental frequency with corresponding harmonics and independent oscillations detected following DFT analysis of time-series photometric data from BN Tri acquired during the TESS Mission (October 8 through October 30, 2019).

	Freq. (c · d^{-1})	*Freq. Err.*	*Amp. (flux)*	*Amp. Err.*	*Phase Err.*	*Phase S/N*	*Amp.*
f_0	14.2789	0.0002	0.0538	0.0043	0.1776	0.0067	767
$2f_0$	28.5578	0.0001	0.0098	0.0001	0.2844	0.0008	128
$3f_0$	42.8367	0.0004	0.0032	0.0001	0.7797	0.0029	58
$4f_0$	57.1156	0.0006	0.0018	0.0001	0.8903	0.0063	32
$5f_0$	71.3922	0.0395	0.0008	0.0002	0.9874	0.1056	14
f_1	14.2502	0.0027	0.0008	0.0038	0.3790	0.0822	11
f_2	25.9221	0.0019	0.0006	0.0001	0.2509	0.0113	10

main-sequence stars were initially targeted for photometric study using two-minute exposures. The TESS CCD detector bandpass ranges between 600 and 1000 nm and is centered near the Cousins I band (I_c). One such BN Tri imaging campaign started on 2019 October 8 and ran every two min through 2019 November 2 but only produced evaluable light curve data during two time segments (2019 October 8–October 15 and 2019 October 21–October 30). Raw flux readings were processed by the TESS Science Processing Operations Center (TESS-SPOC) to remove long term trends using so-called Co-trending Basis Vectors (CBVs). These results identified as "Pre-search Data Conditioning Simple Aperture Photometry" (PDCSAP) flux are usually cleaner data than the SAP flux. A large number (n = 101) of maximum light timings were generated (MAVKA) from the TESS observations. These, along with three more ToMax values interpolated from sparse-sampling surveys (NSVS and ASAS-SN), were used to determine whether any secular changes in the fundamental pulsation period could be detected from the PTD residuals (Table 3).

Since there appeared to be a curvilinear relationship between the ToMax residuals and epoch (Figure 6), near term values (2015–2021) were used to establish an up-to-date linear ephemeris (Equation 1):

$$\text{Max (HJD)} = 2459547.8220(2) + 0{:}0700350(1)\ E. \quad (1)$$

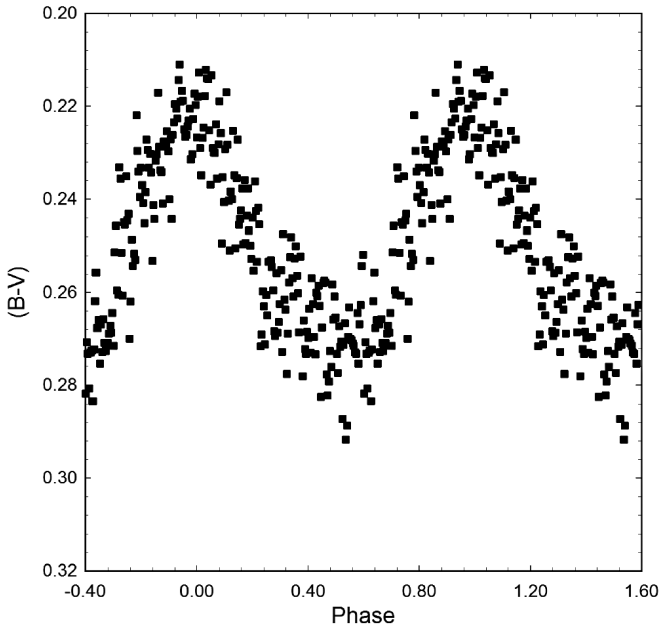

Figure 4. Color curve from BN Tri illustrating significant color change as maximum light B–V≃ 0.22 mag.) descends to minimum light B–V≃ 0.28 mag, where this variable is least bright.

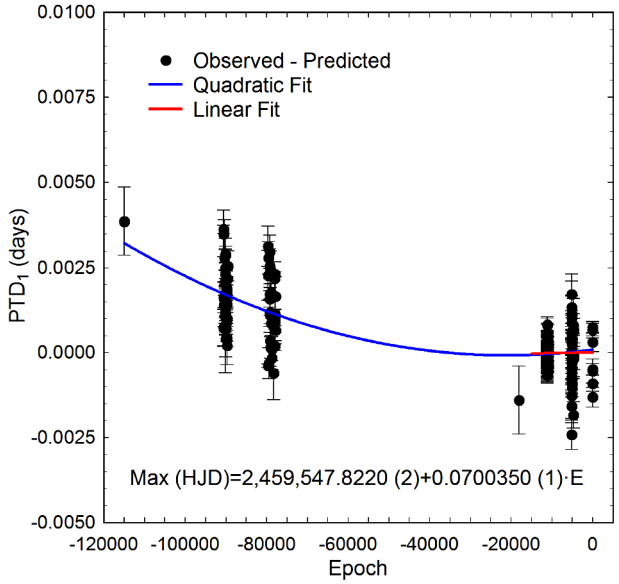

Figure 6. The upwardly directed quadratic fit (Equation 2) to the PTD vs. epoch (cycle number) data is shown with a solid blue line and suggests the pulsation period of BN Tri is increasing with time. The linear ephemeris (Equation 1) was determined from near-term data acquired between 2019 and 2021 (solid red line).

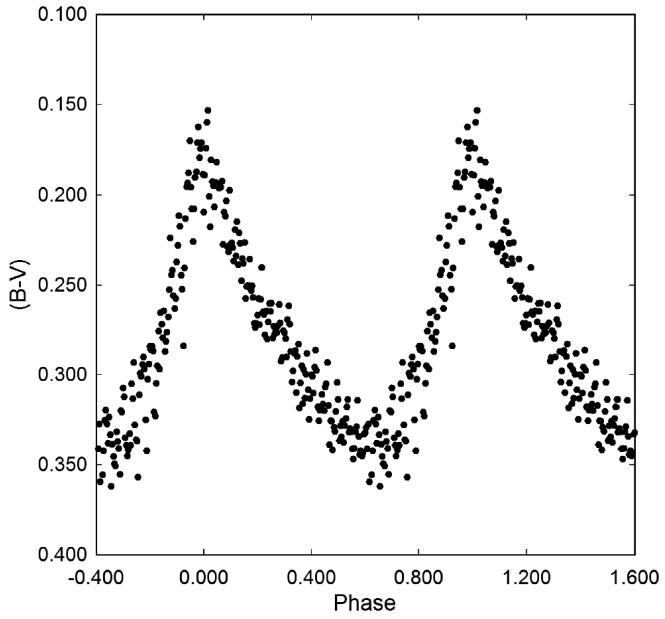

Figure 5. Color curve from V488 Gem illustrating significant color change as maximum light B–V≃ 0.21 mag.) slowly descends to minimum light B–V≃ 0.36 mag.).

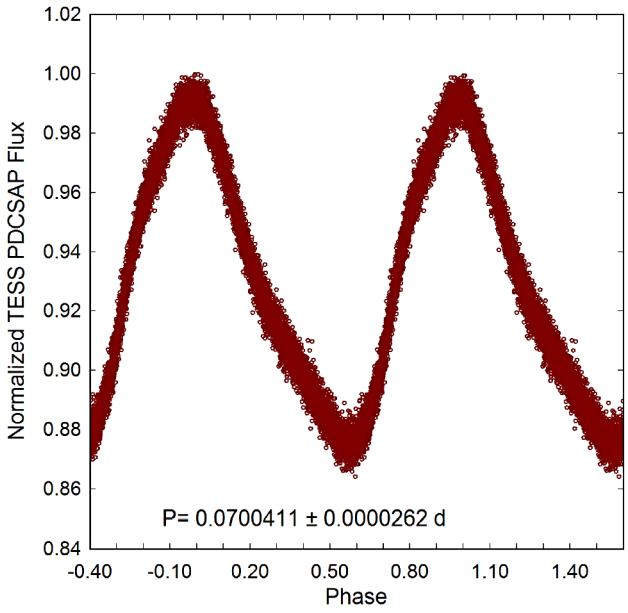

Figure 7. Period (0.0700411 ± 0.0000262 d) folded light curve for BN Tri produced from the TESS Mission between 2019 October 8 and October 30. Data were normalized to maximum light using PDCSAP flux values.

The difference between the observed ToMax times and those predicted by the linear ephemeris (Equation 1) plotted against epoch (cycle number) was best fit by a quadratic relationship (Equation 2) where:

$$\text{Max(HJD)} = 8.8983 \cdot 10^{-5} + 1.5826 \cdot 10^{-8}\,\text{E} + 3.7481 \cdot 10^{-13}\,\text{E}^2. \quad (2)$$

Since the quadratic term coefficient ($+3.7481 \cdot 10^{-13}$) is positive, this result would suggest that the fundamental pulsation period has been slowly increasing with a (1/P) dP/dt value of 5.6 (1.8) · 10^{-8} y^{-1}, a result consistent with observations for Population I radial pulsators (Breger and Pamyanykh 1998). Evolutionary models predict the overwhelming majority should experience increasing periods (Breger and Pamyanykh 1998). In reality there appears to be an equal distribution between period increases and decreases. Pulsation period changes of δ Scuti variables can occur from a variety of evolutionary and non-evolutionary causes (Templeton 2005). These could include undiscovered light-time effects due to binarity, non-linear interactions between pulsation modes, or secular changes in the chemical nature of the star (Neilson *et al.* 2016). Many period changes in δ Scuti systems greatly exceed the rates

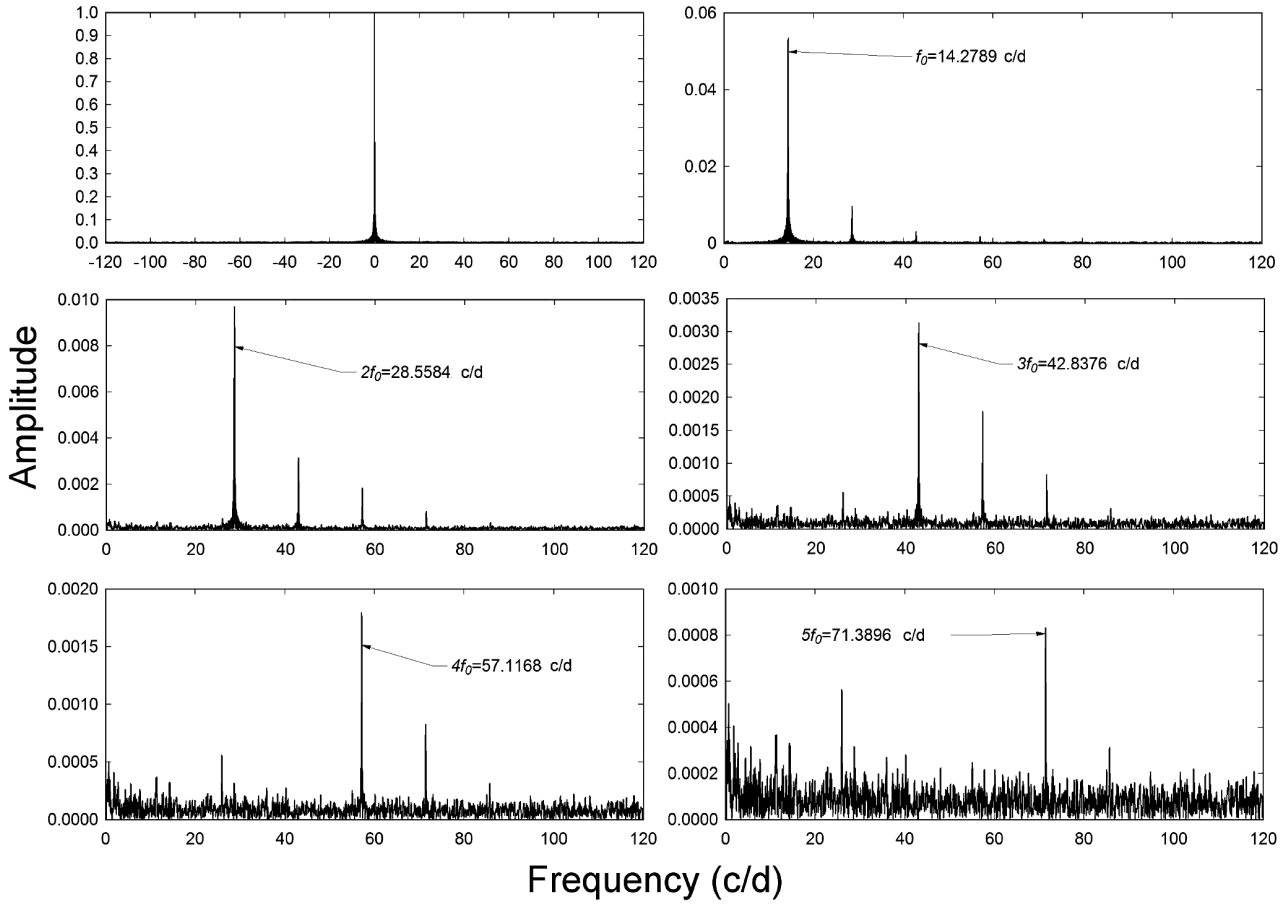

Figure 8. DFT spectral window (top left panel) and amplitude spectra showing the fundamental oscillation frequency (f_0), corresponding harmonics ($2f_0$, $3f_0$, $4f_0$, and $5f_0$), and other independent oscillations (f_1 and f_2) which describe the BN Tri light curves acquired from 2019 October 8 to October 30 during the TESS Mission.

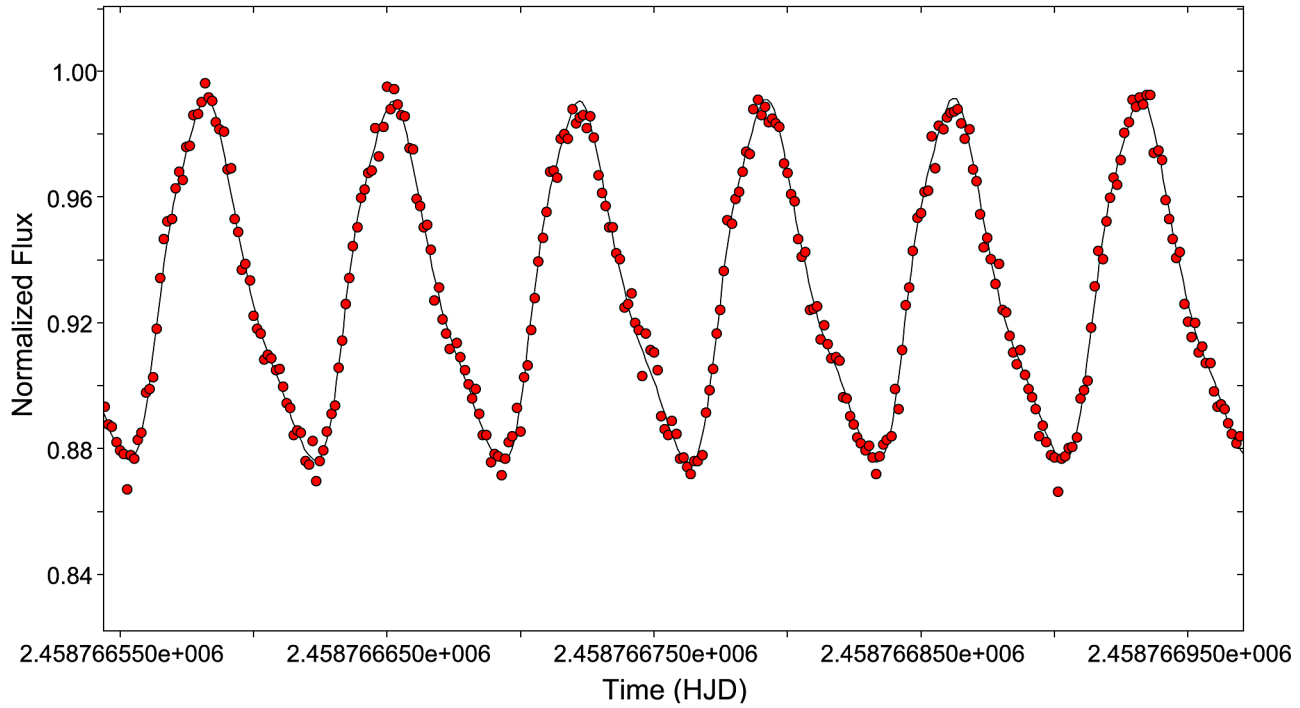

Figure 9. Representative DFT model fit from BN Tri light curve data acquired during TESS Mission (2019 October 10, 01:12 to 10:48 UTC). Observed data are shown as red circles while the DFT-derived simulation is represented with a black line.

Table 5. Global stellar parameters for BN Tri using values reported from observations at DBO and those predicted from evolutionary modelling.

Parameter	*Observed*	*PARSEC (Z = 0.020)*
Mean T_{eff} [K]	7371 ± 186	—[a]
Mass [$M_\odot$]	1.808 ± 0.033	1.759 ± 0.014
Radius [$R_\odot$]	2.185 ± 0.136	2.120 ± 0.021
Luminosity [$L_\odot$]	12.692 ± 0.92	—[a]
rho [g/cm^3]	0.245 ± 0.027	0.260 ± 0.008
log g [cgs]	4.017 ± 0.032	4.031 ± 0.016
Q [d]	0.0292 ± 0.0014	0.0297 ± 0.0011

[a] *T_{eff} and luminosity fixed according to the observed values.*

expected from theoretical models of stellar evolution (Handler 2000; Breger and Pamyatnykh 1998). When the evolutionary model includes the effect from convection core overshoot, improvement between observed rates and model predicted rates was obtained for some but not all stars. The bottom line is that based on current models, evolution alone cannot account for the period changes observed in δ Scuti stars. There may be unknown physical processes at work that the models do not address.

Light curves from BN Tri, and in general other HADS variables, are asymmetrical, characterized by a rapid increase in brightness producing a sharply defined maximum peak. Thereafter a slower decline in magnitude results in a broad minimum. This behavior is commonly observed with pulsating F- to A-type stars. The highly precise flux measurements (PDCSAP $<\pm 0.0038$ $e^- \cdot s^{-1}$) from the TESS satellite revealed very little change in amplitude or light curve morphology (Figure 7) over time.

3.1.2. Discrete Fourier transformation

Discrete Fourier transformation (DFT) was applied using Period04 (Lenz and Breger 2005) to extract statistically significant pulsation frequencies (frequency range = 0–120 $c \cdot d^{-1}$) which best describe the BN Tri light curves. Pre-whitening steps which successively remove the previous most intense signals were employed to draw out other potential oscillations from the residuals. Results derived from BN Tri observations conducted during the TESS Mission (2019 October 8–October 30) are presented in Table 4. A detection limit (S/N ≥ 6) was adopted based on a time-series study with TESS data (Baran and Koen 2021). Uncertainties in frequency, amplitude, and phase were estimated by the Monte Carlo simulation (n = 400) routine featured in Period04. As described above, amplitude-frequency spectra from the TESS Mission (2019 October 8–October 30) are shown in Figure 8, while DFT-derived modelling results indicate a very good fit for the TESS light curve data (Figure 9). Overall, these results are consistent with a HADS variable dominated by a fundamental radial pulsation at $14.2789 \pm 0.0001\ c \cdot d^{-1}$ with potentially two other independent low amplitude pulsations ($f_1 = 14.2502 \pm 0.0001$ and $f_2 = 25.9221 \pm 0.0001\ c \cdot d^{-1}$). The shape of the TESS light curve is best described by harmonics of the fundamental which are detectable up to 5 orders ($2f_0$–$5f_0$). Stellingwerf (1979) defined pulsation modes for δ Scuti stars by calculating the period ratios expected from the first four radial modes. Accordingly the first overtone exists when P_1/P_0 falls between 0.756 and 0.787, the second overtone when P_2/P_0 is between 0.611 and 0.632, and finally the third overtone when P_3/P_0 is between 0.500 and 0.525. Neither f_1 nor f_2 meets the period ratio criteria expected from the first, second, or third radial overtones. They may be artefacts or potentially non-radial modes of oscillation that are becoming increasingly more evident with highly precise photometric measurements of HADS variables taken from space telescopes (Poretti *et al.* 2011).

Fourier deconvolution of light curves (BVI_c) acquired at DBO produced nearly the same fundamental pulsation frequency ($\overline{X} = 14.2786 \pm 0.0001\ c \cdot d^{-1}$) but only revealed statistically significant harmonics at $2f_0$ and $3f_0$. This is testimony to the very high quality of the photometric data acquired by the TESS satellite compared to those produced from ground-based observations.

3.1.3. Global parameters

The Gaia EDR3 parallax-derived distance reported for this variable is 957 ± 16 pc. Since a parallax-derived value is considered the gold-standard for measuring distances, hereafter all calculations dependent on d (pc) use the Gaia EDR3 (Gaia Collab. 2021) value. Absolute V-mag ($M_V = 1.947 \pm 0.078$ mag) was calculated from:

$$M_V = -5 \cdot \log(d) + m - A_V + 5. \quad (3)$$

when $A_V = 0.2567 \pm 0.0059$ mag and $V_{avg} = 12.527 \pm 0.027$ mag. The average V-mag was adopted as a compromise value due to the significant differences between maximum and minimum light.

Luminosity ($12.68 \pm 0.92\ L_\odot$) was determined from:

$$L_* / L_\odot = 10^{((M_{bol\odot} - M_{bol*}) / 2.5)}, \quad (4)$$

When $M_{bol\odot} = 4.74$ mag, $M_V = 1.947 \pm 0.078$ mag, and BC = 0.0338 mag (Flower 1996), then $M_{bol*} = 1.981 \pm 0.078$ mag.

Photometric and spectroscopic observations of eclipsing binary stars are commonly used to determine component mass by applying the laws of gravity and motion derived by Isaac Newton and Johannes Keppler. In contrast, the mass of an isolated field star like BN Tri or V488 Gem is very difficult to determine by direct measurement. However, it is possible under certain conditions to estimate mass according to Eker *et al.* (2018), who empirically derived a mass-luminosity relationship from main sequence (MS) stars in detached binary systems when $1.05 < M_\odot \leq 2.40$. This expression:

$$\log(L) = 4.329(\pm 0.087) \cdot \log(M) - 0.010(\pm 0.019), \quad (5)$$

leads to a mass of $1.808 \pm 0.033\ M_\odot$ for BN Tri. This result, summarized in Table 5 along with others derived from DBO data, is fairly typical for a HADS variable. Finally, the radius ($R_* = 2.185 \pm 0.136\ R_\odot$) was estimated using the well-known relationship where:

$$L_* / L_\odot = (R_* / R_\odot)^2\ (T_* / T_\odot)^4, \quad (6)$$

Values derived for density ($\rho_\odot$), surface gravity (log g), and pulsation constant (Q are also included in Table 5. Stellar density (ρ_*) in g/cm^3 was calculated according to:

$$\rho_* = 3 \cdot M_* \cdot m_\odot / 4\pi (R_* \cdot r_\odot)^3, \quad (7)$$

where $m_\odot$ = solar mass (g), $r_\odot$ = solar radius (cm), M_* is the mass, and R_* the radius of BN Tri in solar units. Using the same algebraic assignments, surface gravity (log g) was determined by the following expression:

$$\log g = \log (M_* \cdot m_\odot \cdot G / (R_* \cdot r_\odot)^2, \quad (8)$$

The dynamical time that it takes a p-mode acoustic wave to internally traverse a star is strongly correlated with the stellar mean density, which can be expressed in terms of other measurable stellar parameters where:

$$\log(Q) = -6.545 + \log(P) + 0.5\log(g) + 0.1M_{bol} + \log(T_{eff}). \quad (9)$$

The full derivation of this expression can be found in Breger (1990). The resulting Q values provided in Table 5 are within the range (Q = 0.025–0.049 d) observed from other δ Sct variables (Breger 1979; Breger and Bregman 1975; North *et al.* 1997; Joshi and Joshi 2015; Antonello and Pastori 1981; Poro *et al.* 2021), where all radial pulsations are derived from the fundamental.

3.1.4. Evolutionary status of BN Tri

The evolutionary status of BN Tri was evaluated (Figure 10) using the PAdova and TRieste Stellar Evolution Code (PARSEC) for stellar tracks and isochrones (Bressan *et al.* 2012) and then plotted (log T_{eff} vs. log($L/L_\odot$)) in a theoretical Hertzsprung-Russell diagram (HRD). The thick solid maroon-colored line defines the zero-age main sequence (ZAMS) position for stars with metallicity Z = 0.020. The two broken lines nearly perpendicular to the ZAMS delimit the blue (left) and red (right) edges of the theoretical instability strip for radial low-p modes (Xiong *et al.* 2016). Also included are the positions of several known HADS and SX Phe-type variables (Balona 2018).

The solid black circle with error bars indicates the fixed position for observed T_{eff} and $L_\odot$ values (Table 5) used to ultimately estimate mass, radius, and age from the PARSEC model when Z = 0.020 or Z = 0.004.

Ironically a single undisputed value for metallicity from the star closest to us remains elusive. Over the last few decades, the reference metallicity values used by several authors for computing stellar models have ranged between Z =0 .012 and 0.020 (Amard *et al.* 2019). Serenelli *et al.* (2016) took great exception to a high solar metallicity value ($Z = 0.0196 \pm 0.0014$) based on in situ measurements of the solar wind (von Steiger and Zurbuchen 2016; Vagnozzi *et al.* 2017) rather than abundance traditionally determined by spectroscopic analysis. Despite the uncertainty in defining an absolute value for $Z_\odot$, an estimate for metal abundance is still required in order to predict the mass, radius, and age of BN Tri from theoretical evolutionary tracks. A Z-value can be estimated indirectly from its location in the Milky Way. According to the following expression:

$$z = d \ \sin(b), \quad (10)$$

the distance in parsecs (z) below or above the Galactic plane can be calculated where $d = 957.12 \pm 15.76$ pc and b is the Galactic latitude (–31.084265°). In this case its position ~500 pc below the Galactic plane suggests residence in the thin disk (Li and Zhao 2017) rather than the halo where many metal poor ([Fe/H] < –1.6) stars like SX Phe-type variables reside (Carollo *et al.* 2010). Furthermore, Qian *et al.* (2018) report an empirical relationship between metallicity ([Fe/H]) and the fundamental pulsation period P) for an NDST star according to the following:

$$[Fe / H] = -0.121(0.026) + 0.92(0.25) \times P. \quad (11)$$

As expected for a thin disk resident, the predicted value ([Fe/H] = -0.056 ± 0.031) suggests that BN Tri approaches solar metallicity, or at most a few times lower.

Two separate PARSEC evolutionary models (Bressan *et al.* 2012) ranging in age between 1×10^8 and 2.21×10^9 y are illustrated in Figure 10. The red solid lines show the model tracks (M_* = 1.70, 1.75, and 1.80 $M_\odot$) over time when Z = 0.020, while the solid blue lines define the metal-poor models (M_* =1.40, 1.45, and 1.50 $M_\odot$) where Z = 0.004. The latter simulations correspond to a decrease in metallicity by a factor of 3 to 5, depending on the reference solar metallicity. Assuming Z =0.020, it can be shown by linear extrapolation that BN Tri would have a mass of 1.759 ± 0.014 $M_\odot$ and a radius of 2.12 ± 0.02 $R_\odot$. The position of this intrinsic variable near the $M_\odot$ = 1.75 evolutionary track extrapolates to an age of 0.996 ± 0.147 Gyr, suggesting it is a moderately evolved MS object lying amongst other HADS variables closer to the blue edge of the instability strip.

By comparison, if BN Tri is more metal deficient (Z = 0.004), then it would have a somewhat greater radius (2.26 ± 0.12 $R_\odot$), but would be less massive (1.44 ± 0.026 $M_\odot$). Its position closest to the 1.45 $M_\odot$ track lies prior to the HRD region where evolutionary tracks of low metallicity stars begin stellar contraction near the end of core hydrogen burning. This star would still be a MS object but with an age approaching 1.96 ± 05 Gyr.

It should be noted that the theoretical mass (1.759 $M_\odot$) where Z = 0.020 is much closer to results (1.773 ± 0.032 $M_\odot$) independently determined using an empirical mass-luminosity relationship. If or when high resolution spectroscopic data become available in the future, uncertainty about the mass and metallicity of BN Tri will likely improve.

3.2. V488 Gem

A total of 330 photometric values in B-, 323 in V-, and 320 in I_c-passbands were acquired at DBO for V488 Gem between 2019 December 21 and 2020 January 18 (Figure 11). Included in these determinations were 25 new ToMax values which are listed in Table 6. ToMax values (n = 79) were determined (MAVKA) from the TESS-SPOC survey (2020 December 31 through 2021 January 13) along with 26 other ToMax values using data mined from the AAVSO VSX archives. An updated linear ephemeris (Figure 12) based on near-term PTD values (2019 December 21–2022 February 7) was derived as follows:

$$\text{Max(HJD)} = 2459618.3444(1) + 0.0932493(1)\ E. \quad (12)$$

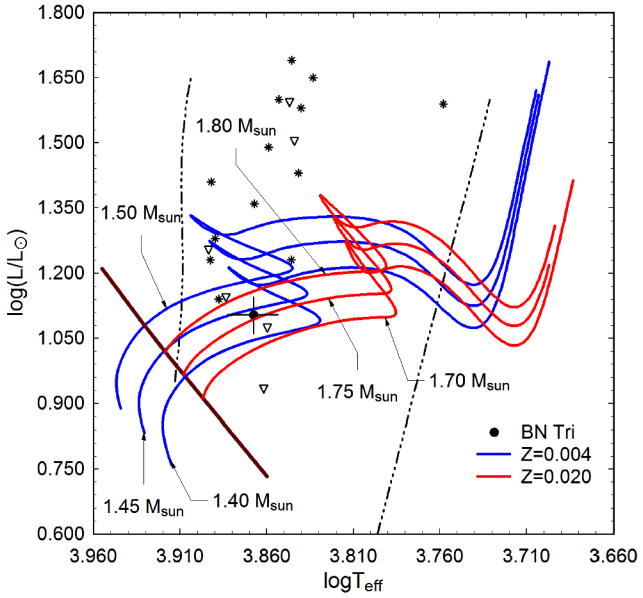

Figure 10. Evolutionary tracks (red lines, Z = 0.020, and blue lines, Z = 0.004) derived from PARSEC models (Bressan *et al.* 2012) showing the position of BN Tri (black filled circle) relative to ZAMS (thick maroon line) and within the theoretical instability strip (black dashed lines) for low-order radial mode δ Scuti pulsators. The position of other HADS (*) and SX Phe (open triangle) variables reported by Balona (2018) are included for comparison.

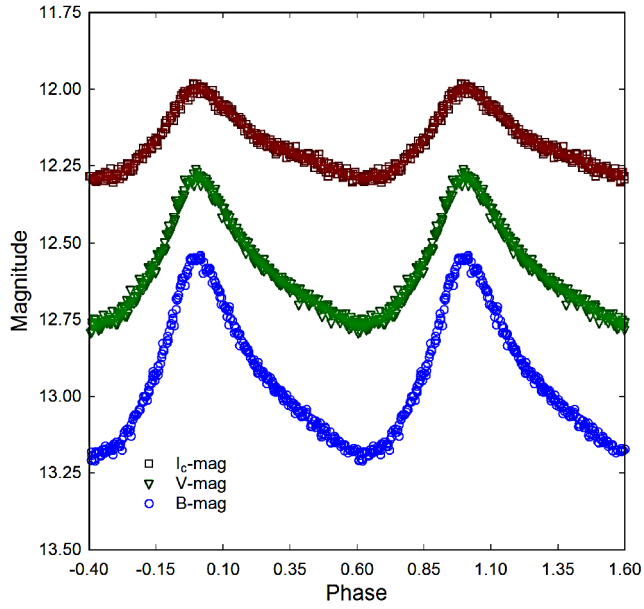

Figure 11. Period (0.093258 ± 0.000001 d) folded CCD light curves for V488 Gem produced from photometric data obtained at DBO between 2019 December 21 and 2020 January 18. The top (I_c), middle (V), and bottom curve (B) shown above were reduced to APASS-based catalog magnitudes using MPO Canopus.

Table 6. Sample table of V488 Gem times-of-maximum (January 31, 2012–February 7, 2022), cycle number and fundamental pulsation timing difference (PTD) between observed and predicted times derived from the updated linear ephemeris (Equation 12).

HJD 2400000+	*HJD Error*	*Cycle No.*	*PTD*	*Ref.*
55958.4130	0.0033	–39249	0.00994	1
56341.3893	0.0015	–35142	0.01141	2
56637.4594	0.0008	–31967	0.01502	2
56656.3897	0.0005	–31764	0.01572	2
59217.4658	0.0001	–4299	0.00010	5
59217.5587	0.0002	–4298	–0.00025	5
59217.6519	0.0002	–4297	–0.00030	5
59217.7463	0.0002	–4296	0.00090	5

References: (1) Wils et al. *(2013); (2) Wils* et al. *(2014); (5) TESS-SPOC (Jenkins* et al. *2016). Full table available at: ftp://ftp.aavso.org/public/datasets/3852-Alton-v488gem.txt. All references relevant to the full table that appears on the AAVSO ftp site are included in the References section of this article and in the full ftp table.*

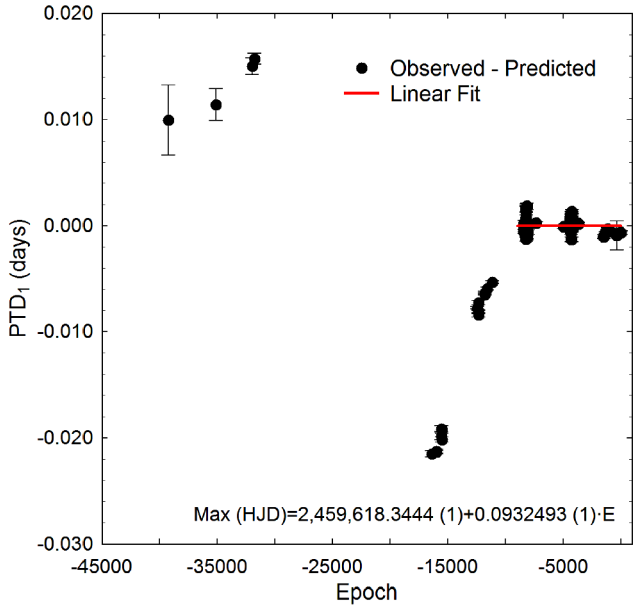

Figure 12. Plot of pulsation timing differences (PTD) vs epoch (cycle number). A linear ephemeris (Equation 12) represented by a solid red line) was determined from near-term (2019–2022) ToMax data.

Table 7. Solution to the putative light-time effect (LiTE) observed from sinusoidal-like changes in V488 Gem fundamental pulsation timings.

Parameter	*Units*	*LiTE values*
HJD0 – 2400000	—	58125.7815 ± 0.0007
P_{orb}	(y)	7.911 ± 0.093
ω	(°)	12.57 ± 1.89
A (semi-ampl.)	(d)	0.0076 ± 0.0001
e	—	0.561 ± 0.027
f(M_2)(mass func.)	($M_\odot$)	0.0612 ± 0.0003
M_2 (i = 90°)	($M_\odot$)	0.811 ± 0.002
M_2 (i = 60°)	($M_\odot$)	0.970 ± 0.002
M_2 (i = 30°)	($M_\odot$)	2.048 ± 0.005
Sum of squared residuals	0.000428	

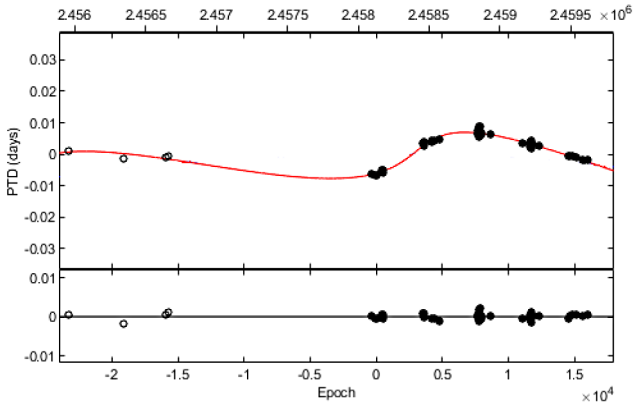

Figure 13. LiTE fit summarized in Table 7 using fundamental pulsation timing differences (PTD) determined for V488 Gem between 2012 January 31 and 2021 February 7. The solid red line in the top panel describes the fit for an elliptical (e = 0.561) orbit (P = 7.911 ± 0.093 y) of a putative binary partner. Solid circles (•) represent the observed times at maximum light. The bottom panel illustrates the PTD residuals remaining after LiTE analysis.

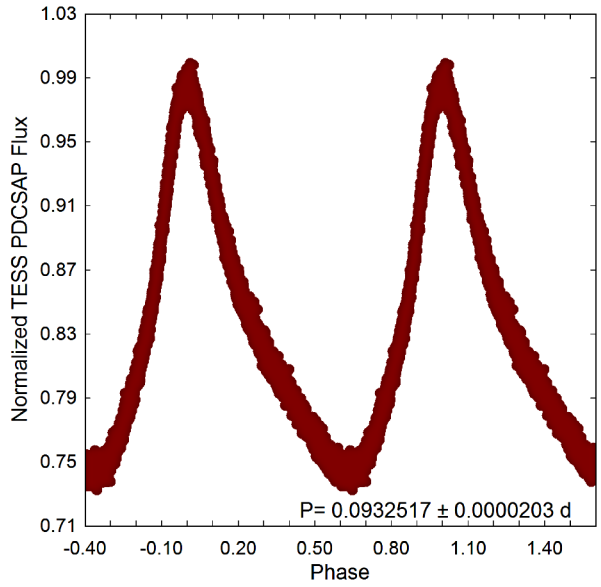

Figure 14. Period (0.0932517 ± 0.0000203 d) folded light curve for V488 Gem produced from the TESS Mission between 2020 December 18 and 2021 January 13. Data were normalized to maximum light using PDCSAP flux values.

Collectively the data suggest complex changes in the apparent fundamental pulsation rate of V488 Gem. One solution posits that cyclic changes in timings for maximum light can result from the gravitational influence of an unseen companion, the so-called light-travel time effect (LiTE). To address this possibility LiTE analyses were performed using an adaptation of the simplex code for third light reported by Zasche *et al.* (2009). Accordingly, the associated parameters in the LiTE equation (Irwin 1959):

$$\rho = \frac{a_{12}\sin i}{c}\left[(1-e^2)\frac{\sin(\nu+\omega)}{1+e\cdot\cos\nu}+\sin\omega\right] \qquad (13)$$

were derived which and include parameter values for P (orbital period of the theoretical binary pair about the barycenter), orbital eccentricity e, argument of periapsis ω, true anomaly

Table 8. Fundamental frequency, corresponding harmonics, and independent oscillations detected following DFT analysis of time-series photometric data from V488 Gem acquired during the TESS Mission (December 18, 2020–January 13, 2021).

	Freq. ($c \cdot d^{-1}$)	*Freq. Err.*	*Amp. (flux)*	*Amp. Err.*	*Phase*	*Phase Err.*	*Amp. S/N*
f_0	10.7233	0.0003	0.09980	0.00324	0.251	0.005	1060
$2f_0$	21.4485	0.0003	0.03456	0.00266	0.828	0.003	629
$3f_0$	32.1717	0.0001	0.01275	0.00004	0.863	0.001	244
$4f_0$	42.8950	0.0001	0.00664	0.00004	0.947	0.001	121
$5f_0$	53.6202	0.0003	0.00335	0.00004	0.510	0.002	67
f_1	10.7506	0.0055	0.00301	0.00307	0.469	0.017	31
$6f_0$	64.3434	0.0005	0.00169	0.00004	0.658	0.004	36
f_2	10.6921	0.0037	0.00137	0.00298	0.709	0.130	14
f_3	10.7837	0.0208	0.00097	0.00007	0.480	0.068	8
$7f_0$	75.0686	0.0009	0.00090	0.00004	0.239	0.007	20
f_0+f_2	21.4212	0.0025	0.00088	0.00266	0.592	0.032	14
f_4	13.3480	0.0012	0.00070	0.00004	0.055	0.009	14

Table 9. Global stellar parameters for V488 Gem using values reported from observations at DBO and those predicted from evolutionary modelling.

Parameter	*Observed*	*PARSEC (Z = 0.020)*
Mean T_{eff} [K]	7129 ± 202	—[a]
Mass [$M_\odot$]	2.152 ± 0.042	2.038 ± 0.036
Radius [$R_\odot$]	3.404 ± 0.232	3.459 ± 0.127
Luminosity [$L_\odot$]	26.97 ± 2.05	—[a]
rho [g/cm^3]	0.077 ± 0.016	0.069 ± 0.008
log g [cgs]	3.707 ± 0.060	3.669 ± 0.033
Q [d]	0.0218 ± 0.0017	0.0209 ± 0.0011

[a] *T_{eff} and luminosity fixed according to the observed values.*

ν, time of periastron passage T_0, and amplitude $A = a_{12} \sin i_2$. Despite a five-year gap in ToMax timings between 2013 and 2018, an eccentric (e = 0.561 ± 0.027) sinusoidal-like fit to these data with very low sum of squared residuals (0.000428) was obtained (Figure 13). The results predict a binary system with an unseen stellar object in an eccentric orbit (7.911 ± 0.093 y) that is located at least 2.97 ± 0.14 AU distant.

The angular resolution of the Gaia photometric detector is limited to 0.18 arcsec (Gaia Collab. 2021). Since the putative secondary is only separated by 2.97 AU (3.36 milli-arcsec), any apparent magnitude determination will be a composite of both stars. The LiTE solution (Table 7) provides three predictions for mass ($M_\odot$), depending on the orbital inclination (90, 60, and 30°). Assuming this nearby star is on the main sequence (MS), then the radius ($R_\odot$) and effective temperature (T_{eff}) can be estimated (Pecaut and Mamajeck 2013). Since the distance is known, the apparent magnitude (V_{mag}) can be calculated. When i = 30°, a secondary with $M_\odot$ = 2.048 would have an apparent V_{mag} of 12.43. Combining the magnitudes from both stars according to:

$$m = m_1 - 2.5\log(1+10^{-0.4(m_2-m_1)}), \qquad (14)$$

reveals that the companion star would brighten the observed V_{mag} (11.60) considerably; therefore, this LiTE prediction when i = 30° is untenable. A less massive companion (0.970 $M_\odot$), such as when the orbital inclination is 60°, is predicted to be

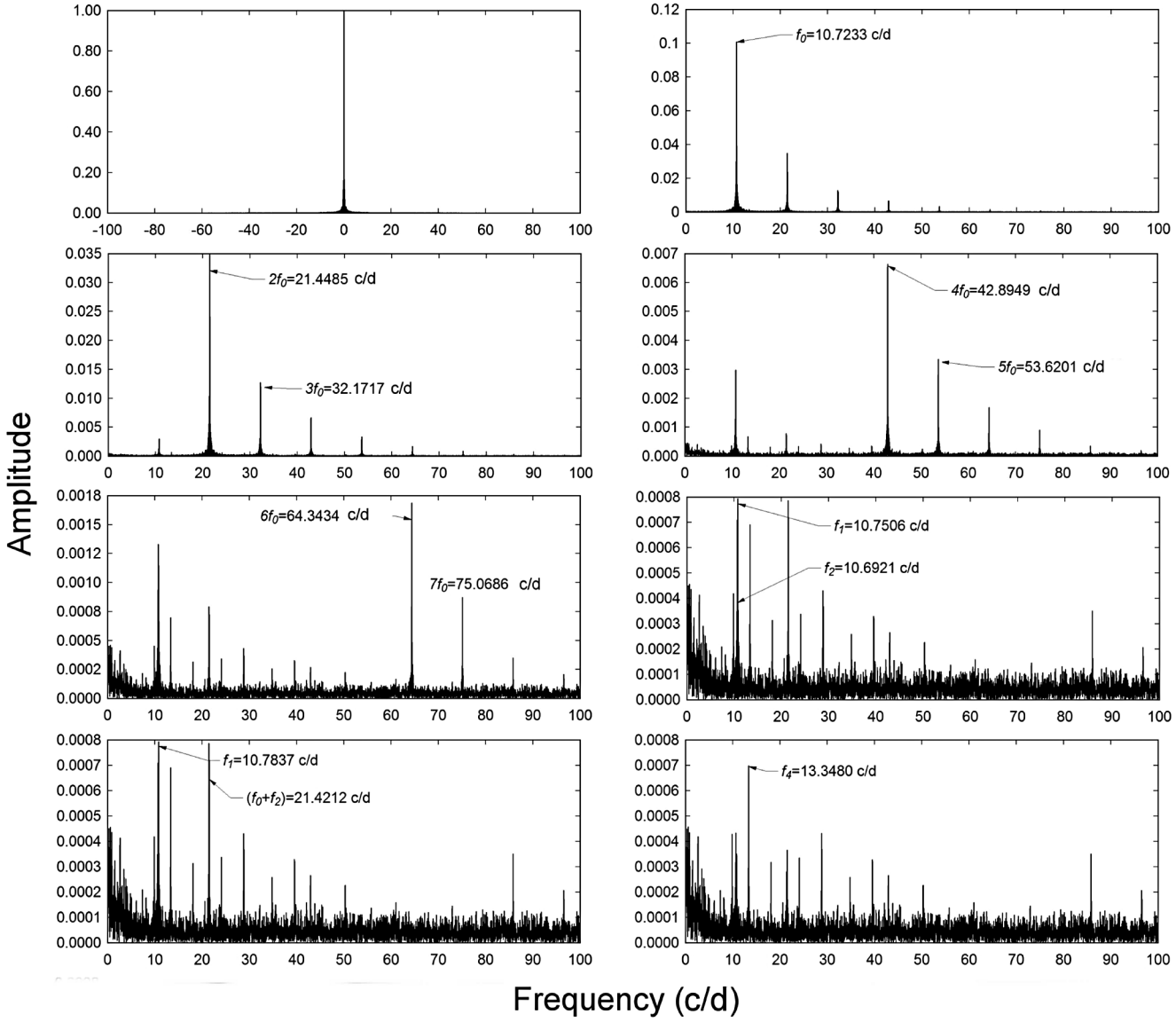

Figure 15. DFT spectral window (top left panel) and amplitude spectra from V488 Gem showing the fundamental pulsation frequency (f_0), its harmonics ($2f_0$–$7f_0$), and independent oscillations (f_i–f_4) from light curves acquired during the TESS Mission (2020 December 18–2021 January 13).

much dimmer (V≃16.02 mag). In this case, the combination of a V≃16.02 mag star with an unresolved V_{avg}≃12.53 mag star would only be slightly brighter (V≃12.48 mag) than the observed value. Said another way, any MS star with an apparent magnitude dimmer than V≃16.02 mag would not meaningfully affect measuring the apparent magnitude of V488 Gem. This analysis constrains the orbital inclination of a putative MS binary partner ($M_\odot$ = 0.811–0.970) to be somewhere between 60 and 90°.

3.2.1 Discrete Fourier transformation

Light curves were mined from the TESS Mission (Ricker *et al.* 2015; Caldwell *et al.* 2020) during an imaging campaign started on 2020 December 18 which ran continuously every two minutes through 2021 January 13. These highly precise flux measurements (PDCSAP < ± 0.0044 $e^- \cdot s^{-1}$) did not reveal any meaningful change over time in amplitude or light curve morphology (Figure 14). As previously described for BN Tri, Period04 (Lenz and Breger 2005) was used to extract prominent frequencies when the frequency range = 0–100 $c \cdot d^{-1}$ (Table 8). Representative amplitude-frequency spectra from the TESS Mission are provided in Figure 15, while DFT-derived modelling results indicate an excellent fit for the TESS light curve data (Figure 16). For the most part, these results suggest that V488 Gem is dominated by a fundamental pulsation at (f_0 = 10.7233 ± 0.0003 $c \cdot d^{-1}$) with a light curve shape that can be best described with harmonics of the fundamental that are detectable up to 7 orders ($7f_0$). In addition, four weak but statistically significant independent oscillations were observed at 10.7506 ± 0.0055 (f_1), 10.6921 ± 0.0037 (f_2), 10.7837 ± 0.0208 (f_3) and 13.3480 ± 0.0012 (f_4) $c \cdot d^{-1}$. One additional pulsation was detected at 21.4212 ± 0.0025 $c \cdot d^{-1}$, which probably represents a combination of f_0 and f_2. It is unlikely that any of these independent oscillations (P_i) correspond to radial overtones based on the calculation of period ratios (P_i / P_0), which did not fit predictions (Stellingwerf 1979). As mentioned

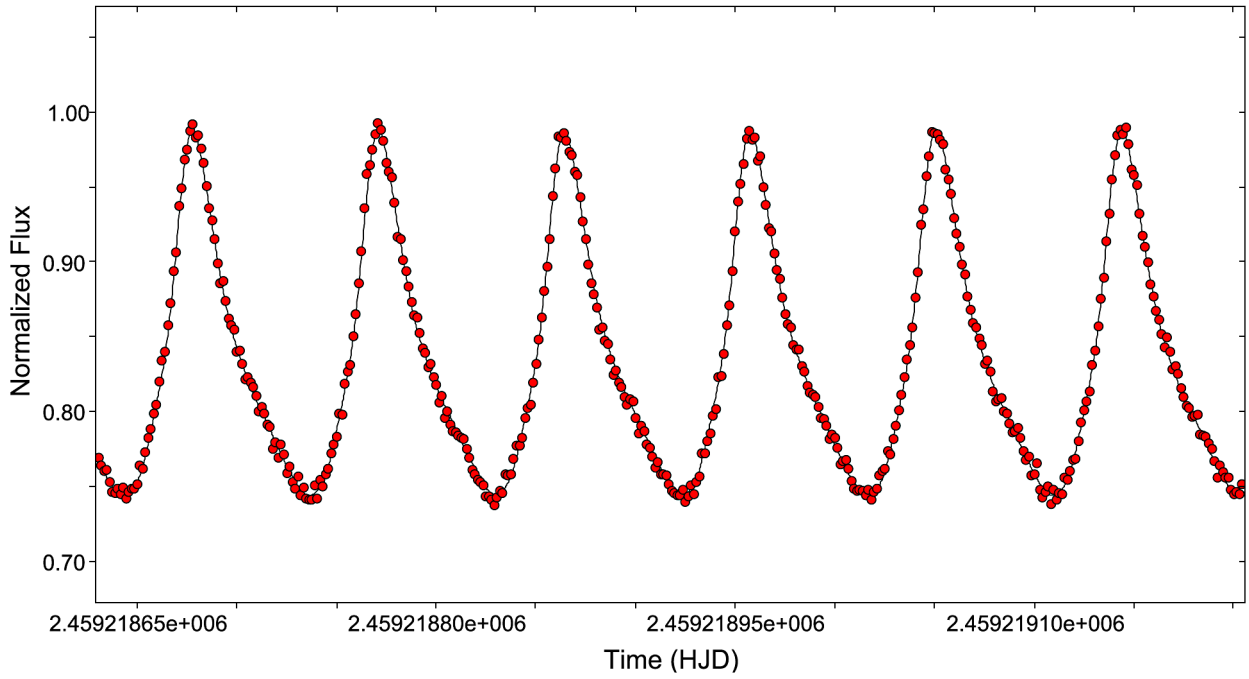

Figure 16. Representative DFT model fit from V488 Gem light curve data acquired during TESS Mission (2021 January 4, 03:06–16:54 UTC). Observed data are shown as red circles while the DFT-derived simulation is represented with a black line.

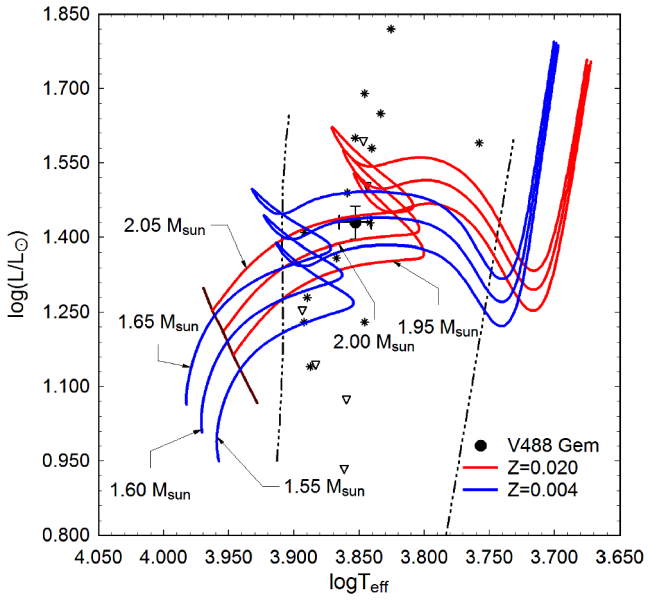

Figure 17. Evolutionary tracks (red lines, Z = 0.020, and blue lines, Z = 0.004) derived from PARSEC models (Bressan *et al.* 2012) showing position of V488 Gem (black filled circle) relative to ZAMS (thick maroon line) and within the theoretical instability strip (black dashed lines) for low-order radial mode δ Scuti pulsators. The position of other HADS (*) and SX Phe (open triangle) variables reported by Balona (2018) are included for comparison.

earlier (section 3.1.2) heretofore undetected pulsation modes continue to be uncovered from the highly precise photometric measurements produced by space telescopes. By comparison, Fourier deconvolution of light curves (BVI_c) acquired at DBO produced nearly the same fundamental pulsation period ($\bar{X}$ = 10.7238 ± 0.0001 c · d^{-1}) and harmonics (2–6f_0) but with no detectable independent modes of oscillation which were probably buried in the periodogram noise.

3.2.2. Global parameters

Estimates for V488 Gem mass, radius, and luminosity in solar units along with density, log g, and Q were derived (Table 9) by applying the same relationships (Equations 3–9) described for BN Tri. Hereafter all calculations dependent on d (pc) use the value reported (1691 ± 61 pc) in Gaia EDR3 (Gaia Collab. 2021). Absolute V-mag (M_V = 1.129 ± 0.083 mag) was calculated from Equation 3 when V_{avg} = 12.527 ± 0.027 mag and A_V =0.2567 ± 0.0059 mag.

As with BN Tri, a mean effective temperature (7129 ± 202 K) for V488 Gem was derived from observations made during this study along with others from various surveys (Table 3). Luminosity (26.97 ± 2.05 $L_\odot$) was determined from Equation 4; when $M_{bol\odot}$ = 4.74 mag, M_V = 1.129 ± 0.083 mag and BC = 0.0334 mag (Flower 1996) then M_{bol*} = 1.163 ± 0.083 mag. Mass (2.152 ± 0.042 $M_\odot$) was estimated from a mass-luminosity relationship (Equation 5) derived from main sequence (MS) stars in detached binary systems (Eker *et al.* 2018). Finally, the radius in solar units (R_* = 3.404 ± 0.232) was estimated using Equation 6. Derived values for density ($\rho_\odot$), surface gravity (log g), and pulsation constant (Q) are also included in Table 9. The resulting Q values provided in Table 9 are lower than the expected (Q = 0.029–0.049 d) value from other δ Sct variables (Breger and Bregman 1975; Breger 1979; Antonello and Pastori 1981; North *et al.* 1997; Joshi and Joshi 2015; Poro *et al.* 2021) known as pure p-mode radial oscillators. This may suggest that one or more of the independent oscillations (f_1–f_4) have affected the pulsation constant. Furthermore, since V488 Gem may have a close binary partner it is uncertain what effect this may have on the determination of Q.

3.2.3. Evolutionary status of V488 Gem

As with BN Tri, the evolutionary status of V488 Gem was evaluated (Figure 17) using the PAdova and TRieste Stellar Evolution Code (PARSEC) for stellar tracks and isochrones (Bressan *et al.* 2012). According to Equation 10, its position ≃230 pc above the Galactic plane suggests residence in the thin disk (Li and Zhao 2017) rather than the halo where many metal-poor ([Fe/H] <–1.6) stars reside (Carollo *et al.* 2010). As expected for a thin disk denizen, the LAMOST spectroscopic value ([Fe/H] = –0.237 ± 0.056) suggests that V488 Gem approaches (~58%) solar metallicity.

Separate PARSEC evolutionary models (Bressan *et al.* 2012) ranging in age between 1.013×10^8 and 1.63×10^9 y are illustrated in Figure 17. The solid black circle with error bars indicates the HRD position when fixed by the observed T_{eff} and $L_{\odot}$ values (Table 9). If Z = 0.020, then by linear extrapolation V488 Gem would have a mass of 2.038 ± 0.036 $M_{\odot}$ and a radius of 3.459 ± 0.127 $R_{\odot}$. The position of this intrinsic variable closest to the $M_{\odot}$ = 2.05 evolutionary track extrapolates to an age of 1.013 ± 0.020 Gyr, suggesting it is a moderately evolved MS object lying amongst other HADS variables closer to the blue edge of the instability strip.

By comparison, a metal-deficient (Z = 0.004) V488 Gem would have a slightly smaller radius (3.425 ± 0.148 $R_{\odot}$), but would be considerably less massive (1.593 ± 0.030 $M_{\odot}$). Its position near the 1.60 $M_{\odot}$ track lies after the HRD region where evolutionary tracks of low metallicity stars begin stellar contraction near the end of core hydrogen burning. This star would still be a MS object but with an age approaching 1.613 ± 0.001 Gyr. It should be noted that the theoretical mass (2.038 $M_{\odot}$) where Z = 0.020 favors the higher metallicity of V488 Gem is also in general agreement with results (2.152 ± 0.042 $M_{\odot}$) independently determined using an empirical mass-luminosity relationship (Equation 5). Uncertainty about the mass and metallicity of V488 Gem will likely improve should high resolution spectroscopic data become available in the future.

4. Conclusions

New times of maximum were determined for both BN Tri and V488 Gem based on precise time-series CCD-derived light curve data acquired at DBO. These along with other published values and those extracted from the SuperWASP (Pollacco *et al.* 2006) and TESS (Ricker *et al.* 2015; Caldwell *et al.* 2020) surveys led to an updated linear ephemeris for each system. Potential changes in the fundamental pulsation period were assessed using differences between observed and predicted timings for maximum light. A quadratic relationship was established between the residuals and epoch for BN Tri, suggesting that the pulsation period appears to be very slowly increasing (0.0003 ± 0.0001 s · y^{-1}). Secular analysis of the fundamental pulsation period for V488 Gem revealed a sinusoidal-like variation in the pulse timing differences over a nine year period. These residuals, believed to result from a light-travel time effect, were fit using simplex optimization and subsequently suggest that V488 Gem is a binary system with a stellar-sized companion in an eccentric orbit (7.91 y). Continued observation of both systems for at least a decade could prove highly useful in affirming their secular behavior. The adopted effective temperatures (T_{eff}) for BN Tri (7371 ± 186 K) and V488 Gem (7129 ± 202 K) most likely correspond to spectral class A8V-F0V for the former and A9V-F1V for the latter variable. The totality of results, including residence in the Galactic thin disk, near solar metallicity, mass predictions, and effective temperature estimates, firmly support classification for both stars as HADS-type variables. Nonetheless, high resolution UV-vis spectra would be necessary to unequivocally confirm the spectral type, metallicity, and effective temperature of both systems.

5. Acknowledgements

This research has made use of the SIMBAD database operated at Centre de Données astronomiques de Strasbourg, France. In addition, the Northern Sky Variability Survey previously hosted by the Los Alamos National Laboratory, and the ASAS-SN Variable Stars Database (https://asas-sn.osu.edu/variables) were mined for essential information. This work also presents results from the European Space Agency (ESA) space mission Gaia (DR2 and EDR3). Gaia data are processed by the Gaia Data Processing and Analysis Consortium (DPAC). Funding for the DPAC is provided by national institutions, in particular those participating in the Gaia MultiLateral Agreement (MLA). The Gaia mission website is https://www.cosmos.esa.int/gaia. The Gaia archive website is https://archives.esac.esa.int/gaia. This paper makes use of data from the first public release of the WASP data as provided by the WASP consortium and services at the National Aeronautics and Space Administration (NASA) Exoplanet Archive, which is operated by the California Institute of Technology, under contract with NASA under the Exoplanet Exploration Program. The use of public data from the Large Sky Area Multi-Object Fiber Spectroscopic Telescope (LAMOST) is also acknowledged. Guoshoujing Telescope is a National Major Scientific Project built by the Chinese Academy of Sciences. Funding for the project has been provided by the National Development and Reform Commission. LAMOST is operated and managed by the National Astronomical Observatories, Chinese Academy of Sciences. Some of the data presented in this paper were obtained from the Mikulski Archive for Space Telescopes (MAST) at the Space Telescope Science Institute. Support to MAST for these data is provided by the NASA Office of Space Science via grant NAG57584 and by other grants and contracts. This paper also includes data collected with the TESS mission, obtained from the MAST data archive at the Space Telescope Science Institute (STScI). Funding for the TESS mission is provided by the NASA Explorer Program. STScI is operated by the Association of Universities for Research in Astronomy, Inc., under NASA contract NAS 526555. Many thanks to the anonymous referee whose valuable commentary and corrections led to significant improvement of this paper. This research was made possible through use of the AAVSO Photometric All-Sky Survey (APASS), funded by the Robert Martin Ayers Sciences Fund.

References

Akerlof, C., *et al.* 2000, *Astron. J.*, **119**, 1901.

Amard, L., Palacios, A., Charbonnel, C., Gallet, F., Georgy, C., Lagarde, N., and Siess, L. 2019, *Astron. Astrophys.*, **631A**, 77.

Andrych, K. D., and Andronov, I. L. 2019, *Open Eur. J. Var. Stars*, **197**, 65.

Andrych, K. D., Andronov, I. L., and Chinarova, L. L. 2020, *J. Phys. Stud.*, **24**, 1902.

Antonello, E., and Pastori, L. 1981, *Publ. Astron. Soc. Pacific*, **93**, 237.

Baglin, A. 2003, *Adv. Space Res.*, **31**, 345.

Balona, L. A. 2018, *Mon. Not. Roy. Astron. Soc.*, **479**, 183.

Balona, L. A., and Nemec, J .M. 2012, *Mon. Not. Roy. Astron. Soc.*, **426**, 2413.

Baran, A. S., and Koen, C. 2021, *Acta Astron.*, **71**, 113.

Berry, R. and Burnell, J. 2005, *The Handbook of Astronomical Image Processing*, 2nd ed., Willmann-Bell, Richmond VA.

Breger, M. 1979, *Publ. Astron. Soc. Pacific*, **91**, 5.

Breger, M. 1990, *Delta Scuti Star Newsl.*, **2**, 13.

Breger, M., and Bregman, J. N. 1975, *Astrophys. J.*, **200**, 343.

Breger, M., and Pamyatnykh, A. A. 1998, *Astron. Astrophys.*, **332**, 958.

Bressan, A., Marigo, P., Girardi, L., Salasnich, B., Dal Cero, C., Rubele, S., and Nanni, A. 2012, *Mon. Not. Roy. Astron. Soc.*, **427**, 127.

Caldwell, D. A. 2020, *Res. Notes Amer. Astron. Soc.*, **4**, 201.

Carollo, D., *et al.* 2010, *Astrophys. J.*, **712**, 692.

Drake, A. J., *et al.* 2014, *Astrophys. J., Suppl. Ser.*, **213**, 9.

Eker, Z., *et al.* 2018, *Mon. Not. Roy. Astron. Soc.*, **479**, 5491.

Flower, P. J. 1996, *Astrophys. J.*, **469**, 355.

Gaia Collaboration, *et al.* 2016, *Astron. Astrophys.*, **595A**, 1.

Gaia Collaboration, *et al.* 2018, *Astron. Astrophys.*, **616A**, 1.

Gaia Collaboration, *et al.* 2021, *Astron. Astrophys.*, **649A**, 1.

Garg, A., *et al.* 2010, *Astron. J.*, **140**, 328.

Gettel, S. J., Geske, M. T., and McKay, T. A. 2006, *Astron. J.*, **131**, 621.

Gilliland, R. L., *et al.* 2010, *Publ. Astron. Soc. Pacific*, **122**, 131.

Guzik, J. A. 2021, *Frontiers Astron. Space Sci.*, **8**, 1.

Handler, G. 2000, in *The Impact of Large-Scale Surveys on Pulsating Star Research*, eds. L. Szabados, D. Kurtz, ASP Conf. Ser. 203, Astronomical Society of the Pacific, San Francisco, 408.

Henden, A. A., Levine, S. E., Terrell, D., Smith, T. C., and Welch, D. L. 2011, *Bull. Amer. Astron. Soc.*, **43**.

Henden, A. A., Terrell, D., Welch, D., and Smith, T. C. 2010, *Bull. Amer. Astron. Soc.*, **42**, 515.

Henden, A. A., Welch, D. L., Terrell, D., and Levine, S. E. 2009, *Bull. Amer. Astron. Soc.*, **41**, 669.

Irwin, J. B. 1959, *Astron. J.*, **64**, 149.

Jayasinghe, T., *et al.* 2018, *Mon. Not. Roy. Astron. Soc.*, **477**, 3145.

Jenkins, J. M., *et al.* 2016, *Proc. SPIE*, **9913**, id. 99133E.

Jester, S., *et al.* 2005, *Astron. J.*, **130**, 873.

Joshi, S., and Joshi, Y. C. 2015, *J. Astrophys, Astron.*, **36**, 33.

Kafka, S. 2021, Observations from the AAVSO International Database (https://www.aavso.org/data-download).

Khruslov, A.V. 2007, *Perem. Zvezdy Prilozh.*, **7**, 25.

Lee, Y.-H, Kim, S. S., Shin, J., Lee, J., and Jin, H. 2008, *Publ. Astron. Soc. Japan*, **60**, 551.

Lenz, P., and Breger, M. 2005, *Commun. Asteroseismology*, **146**, 53.

Li, C., and Zhao, G. 2017, *Astrophys. J.*, **850**, 25.

McNamara, D. H. 2000, in *Delta Scuti and Related Stars, Reference Handbook and Proceedings of the 6th Vienna Workshop in Astrophysics*, eds. M. Breger, M. Montgomery, ASP Conf. Ser. 210, Astronomical Society of the Pacific, San Francisco, 373.

McNamara, D. H. 2011, *Astron. J.*, **142**, 110.

Minor Planet Observer. 2010, MPO Software Suite (http://www.minorplanetobserver.com), BDW Publishing, Colorado Springs.

Mortara, L., and Fowler, A. 1981, in *Solid State Images for Astronomy*, SPIE Conf. Proc. 290, 28, Society for Photo-Optical Instrumentation Engineers, Bellingham, WA, 28.

Neilson, H. R., Percy, J. R., and Smith, H. A. 2016, *J. Amer. Assoc. Var. Star Obs.*, **44**, 179.

Niu, J.-S, Fu, J.-N., and Zong, W.-K. 2013, *Res. Astron. Astrophys.*, **13**, 1181.

Niu, J.-S, *et al.* 2017, *Mon. Not. Roy. Astron. Soc.*, **467**, 3122.

North, P., Jaschek, C., and Egret, D. 1997, *Proceedings of the ESA Symposium "Hipparcos-Venice '97,"* ESA SP-402, ESA Publications Division, Noordwijk, The Netherlands, 367.

Pamyatnykh, A. A. 1999, *Acta Astron.*, **49**, 119.

Pecaut, M. J., and Mamajek, E. E. 2013, *Astrophys. J., Suppl. Ser.*, **208**, 9.

Pojmański, G. 2000, *Acta Astron.*, **50**, 177.

Pojmański, G., Pilecki, B., and Szczygiel, D. 2005, *Acta Astron.*, **55**, 275.

Pollacco, D. L., *et al.* 2006, *Publ. Astron. Soc. Pacific*, **118**, 1407.

Poretti, E. 2003a, *Astron. Asstrophys.*, **409**, 1031.

Poretti, E. 2003b, in *Interplay of Periodic, Cyclic and Stochastic Variability in Selected Areas of the H-R Diagram*, ed. C. Sterken, ASP Conf. Ser. 292, Astronomical Society of the Pacific, San Francisco, 145.

Poretti, E., *et al.* 2011, *Astron. Astrophys.*, **528A**, 147.

Poro, A., *et al.* 2021, *Publ. Astron. Soc. Pacific*, **133**, 084201.

Qian, S.-B., Li, L.-J., He, J.-J., Zhang, J., Zhu, L.-Y., and Han, Z.-T. 2018, *Mon. Not. Roy. Astron. Soc.*, **475**, 478.

Ricker, G., *et al.* 2015, *J. Astron. Telesc. Instrum. Syst.*, **1**, 014003.

Schlafly, E. F., and Finkbeiner, D. P. 2011, *Astrophys. J.*, **737**, 103.

Serenelli, A., Scott, P., Villante, F. L., Vincent, A. C., Asplund, M., Basu, S., Grevesse, N., and Peña-Garay, C. 2016, *Mon. Not. Roy. Astron. Soc.*, **463**, 2.

Smith, T. C., Henden, A. A., and Starkey, D. R. 2011, in *The Society for Astronomical Sciences 30th Annual Symposium on Telescope Science*, Society for Astronomical Sciences, Rancho Cucamonga, CA, 121.

Software Bisque. 2019, TheSkyX Professional Edition 10.5.0 (https://www.bisque.com).

Stellingwerf, R. F. 1979, *Astrophys. J.*, **227**, 935.
Templeton, M. R. 2005, *J. Amer. Assoc. Var. Star Obs.*, **34**, 1.
Vagnozzi, S., Freese, K, and Zurbuchen, T. H. 2017, *Astrophys. J.*, **839**, 55.
von Steiger, R., and Zurbuchen, T. H. 2016, *Astrophys. J.*, **816**, 13.
Walker, G., *et al.* 2003, *Publ. Astron. Soc. Pacific*, **115**, 1023.
Wils, P., *et al.* 2013, *Inf. Bull. Var. Stars*, No. 6049, 1.
Wils, P., *et al.* 2014, *Inf. Bull. Var. Stars*, No. 6122, 1.
Woźniak, P. R., *et al.* 2004, *Astron. J.*, **127**, 2436.
Xiong, D. R., Deng, L., Zhang, C., and Wang, K. 2016, *Mon. Not. Roy. Astron. Soc.*, **457**, 3163.
Zasche, P., Liakos, A., Niarchos, P., Wolf, M., Manimanis, V., and Gazeas, K. 2009, *New Astron.*, **14**, 121.
Zhao, G., Zhao, Y.-H., Chu, Y.-Q., Jing, Y.-P., and Deng, L.-C. 2012, *Res. Astron. Astrophys.*, **12**, 723.